The Hitchhiker's Guide to the Periplasm:

Unexpected Molecular Interactions of Antibiotics

Revealed by Considering Crowding Effects in *E. coli*

Conrado Pedebos[1], Iain P. S. Smith[1], Alister Boags[1,2], Syma Khalid[1*]

[1]School of Chemistry, University of Southampton, Highfield Campus, Southampton
SO17 1BJ, UK
[2]Bioinformatics Institute (A*STAR), 30 Biopolis Street, #07-01 Matrix, Singapore
138671, Singapore

*To whom correspondence should be addressed. E-mail: S.Khalid@soton.ac.uk

27

28

Abstract

The periplasm of Gram-negative bacteria is a highly crowded environment comprised of many different molecular species. Antibacterial agents that causes lysis of Gram-negative bacteria by their action against the inner membrane must cross the periplasm to arrive at their target membrane. Very little is currently known about their route through the periplasm, and the interactions they experience. To this end, here atomistic molecular dynamics simulations are used to study the path taken by the antibiotic polymyxin B1 through a number of models of the periplasm which are crowded with proteins and osmolytes to different extents. The simulations reveal that PMB1 forms transient and long-lived interactions with proteins and osmolytes that are free in solution as well as lipoproteins anchored to the outer membrane and bound to the cell wall. We show that PMB1 may be able to 'hitchhike' within the periplasm by binding to lipoprotein carriers. Overall our results show that PMB1 is rarely uncomplexed within the periplasm; an important consideration for interpretations of its therapeutic mechanism of action. It is likely that this observation can be extended to other antibiotics that rely on diffusion to cross the periplasm.

45

46

47

48

49

50

51

52

53

54

55

56

57

58

59

60

Introduction

The periplasm of Gram-negative bacteria is a crowded aqueous compartment bounded by the inner and outer membranes. The cell wall is contained within the periplasm as well as hundreds of proteins including chaperones, transporters proteases and nucleases[1,2]. The solution also contains a range of osmolytes, including urea, sugars, spermidine and putrescine. This makes for a complex and crowded environment for any molecular species to negotiate when moving across the periplasm towards either membrane. Very little is known about the spatial arrangement of these myriad molecules within the periplasm. In other words, it is not known if the proteins and osmolytes are evenly distributed, or if is there some degree of organization and if so, to what extent. This makes it very difficult to predict the interactions experienced by molecules within the periplasm. This extends to molecules that are not native to the bacteria, such as antibacterial agents. Thus, we have little information regarding which moieties of antibiotics are available to carry out the desired functions, and which are unavailable as they are involved in interactions with native proteins/osmolytes/cell wall. To this end we have conducted a study of polymyxin B1 (PMB1) within models of the *E. coli* periplasm. PMB1 is a lipopeptide antibiotic used as a "last resort" drug for the treatment of infections caused by Gram-negative bacteria[3]. PMB is composed of a cyclic, cationic polypeptide ring connected to a branched fatty acid tail. The cationic ring contains five residues of the irregular amino acid α,γ-Diamino Butyric acid (DAB), each of which contributes a charge of +1 e giving PMB1 an overall charge of +5 e. The cationic ring enables solubility in aqueous solvents, whereas the lipid tail facilitates insertion into bacterial membranes[4-7]. While PMB1 along with colistin (polymyxin E) were for many years, last resort antibiotics, in recent years bacterial strains that are resistant to both antibiotics have emerged in a number of countries[8,9]. Thus, in order to either modify these drugs or to develop completely novel antibiotics, it is timely to establish a thorough, molecular-level understanding of each stage of the process *via* which they bring about bacterial cell death. To date, mechanistic studies of PMB1 have focused almost entirely on the two

4

90   membranes of Gram-negative bacteria[7,10], leaving unaddressed the question, how does

91   PMB1 cross the periplasm to get from the outer membrane to the inner membrane?

92   Here, a series of atomistic molecular dynamics simulations (Table 1) were performed of

93   models of portions of the *E. coli* cell envelope. The simulation systems contain an

94   asymmetric model of the outer membrane composed of LPS and phospholipids, a single-

95   layered cell wall, various proteins/lipoproteins, osmolytes and PMB1, with systems sizes

96   ranging from 200,000 to 750,000 atoms. The proteins are a combination of Braun's

97   lipoprotein (BLP), LolA, LolB, OmpA, and Pal (Fig1). BLP is the most abundant protein in

98   *E. coli* (there are an estimated 10^5 copies of BLP in each *E. coli*[11]). It exists as a coiled-

99   coil trimer that is essential for compartment stability[12]. It is anchored in the outer

100 membrane *via* a lipidated moiety at its N-terminus, whereas it is covalently bound to

101 peptidoglycan via its C-terminus. LolA and LolB are small soluble proteins that carry

102 lipoproteins[13,14], they are largely similar in structure, although LolB is anchored to the OM

103 *via* a lipidated moiety whereas LolA is free to diffuse across the cell envelope. OmpA is

104 composed of an eight-stranded barrel which is located in the OM, and is connected *via* a

105 linker to the soluble domain that can bind peptidoglycan in the periplasm[15,16,17]. Pal also

106 has a lipidated anchor in the OM like LolB, while its C-terminal domain resembles the

107 OmpA soluble domain. Like OmpA, Pal also has a linker that can extend into the

108 periplasm enabling the protein to bind non-covalently to peptidoglycan, thereby assisting

109 with maintaining compartment integrity[18,19]. Where present, in each system there are 4 x

110 BLPs and 1 x each of OmpA, Pal, LolA and LolB. The most compositionally complex

111 system studied here also contained a range of osmolytes, in order to better represent the

112 crowded environment that these molecules encounter in the periplasm.

113 The osmolytes incorporated into our periplasmic model were selected on the basis of a

114 combination of their abundance and chemical diversity. Importantly, all of these osmolytes

115 have their concentrations in the periplasm either documented or estimated in the

116 literature[20-25] and these concentrations are reproduced here: osmoregulated periplasmic

117 glucans (OPG) (20 mM), trehalose (10 mM), putrescine (30 mM), spermidine (3 mM),

118 glycerol (36 mM) and urea (20 mM). Both OPG and trehalose are widely distributed in

119 Bacteria, with OPG having a prominent role on regulating osmotic pressure and

120 virulence[26], whereas trehalose is mainly involved in response to stress conditions[27]. The

121   polyamines, putrescine and spermidine, are the two most common in all bacteria, with

122   functions that includes supporting bacterial growth, incorporation into the cell wall, and

123   biosynthesis of siderophores[28]. Glycerol is metabolized in *E. coli* cells for different

124   applications, both aerobically and anaerobically[29,30]. Urea is a source of nitrogen, after its

125   breakdown[31].

126   Simulations were initiated by placing PMB1 molecules randomly in the aqueous region

127   between the outer membrane and the cell wall. The osmolyte concentrations are derived

128   from literature values and the number of proteins is selected to reproduce crowding

129   volume fraction of ϕ ~0.21 as estimated from experimental studies[20]. A set of simulations

130   of PMB1 in just water and ions was also performed for comparison.

131

132   **Results**

133   Table 1 provided a summary of the simulations performed in this study. Initial

134   observations focused on general mobility and aggregation of PMB1 followed by in depth

135   analyses probing the causes of these observations.

136

137   **Table 1.** Summary of all simulated systems.

Simulations					
System	Proteins	PMB1 Molecules	Osmolytes and Ions[a]	Length	Force field
PMB$_{only}$	None	30	Na$^+$, Cl$^-$	1 μs	GROMOS 54a7
PMB$_{dil}$	BLP (x4)	30	Na$^+$, Cl$^-$	2 x 500 ns	GROMOS 54a7
PMB$_{prot}$	BLP (x4), LolA, LolB, Pal, OmpA	30	Na$^+$, Cl$^-$	2 x 500ns	GROMOS 54a7
PMB$_{crowd}$	BLP (x4), LolA, LolB, Pal, OmpA	30	Na$^+$, Cl$^-$, Glycerol, Urea, Trehalose, Spermidine, Putrescine, OPG	2 x 500 ns	GROMOS 54a7

138   [a] Molar concentration: Na+, Cl- (200 mM), Glycerol (35mM), Urea (30mM), Trehalose (10 mM), Spermidine (0.2 mM),
139   Putrescine (30 mM), Osmoregulated Periplasmic Glucans (OPG - 20 mM).

140

141   The crowded nature of the systems had a clear impact upon the solvent accessible

142   surface area (SASA) of PMB1 (Fig. 1). The SASA is lower when PMB1 molecules are just

143   in water and counter ions (PMB1$_{only}$), compared to when in the protein-containing systems

144   (PMB1$_{dil}$, PMB1$_{prot}$ and PMB1$_{crowd}$). Tracking the PMB1 motion within the XY plane (Fig.

145   S1) of the protein-containing systems shows the movement of polymyxins in the crowded

146   systems (PMB1$_{crowd}$ and PMB1$_{prot}$) is more confined compared to PMB1$_{dil}$ in which BLP

147   is the only protein. Additionally, in the latter system, more PMB1 molecules moved

148   towards the outer membrane and the cell wall rather than remaining in the solution area

149   between these two large structures, compared to PMB1$_{crowd}$ and PMB1$_{prot}$. Another effect

150   observed with increasing system complexity is the slower diffusion of PMB1 (Fig. 2A and

151   Fig. S2), by calculation of the translational diffusion coefficients (D_t) from two different

152   time regimes (1-10ns; and 50-100ns). For the PMB$_{only}$ system, the D_t from the longer time

153   regime was estimated to be $4.0 \pm 0.3 \times 10^{-6}$ cm^2/s, while for PMB$_{dil}$, PMB$_{prot,}$ and PMB$_{crowd}$

154   systems, the values were $3.8 \pm 0.4 \times 10^{-8}$ cm^2/s, $2.9 \pm 0.3 \times 10^{-8}$ cm^2/s and $2.0 \pm 0.4 \times 10^{-8}$

155   ^{8} cm^2/s, respectively, demonstrating a major reduction when compared to PMB$_{only}$ (100-

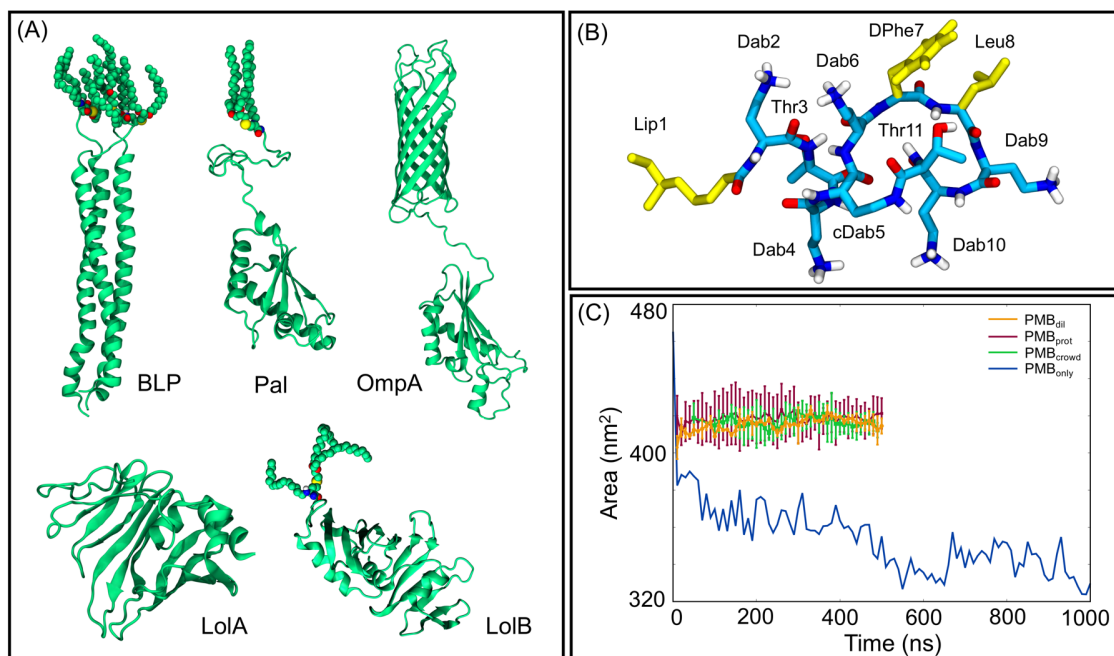156   fold). The slowest diffusion is recorded for the most crowded system.

157

158   **Figure 1. Summary of proteins studied and SASA data. Panel (A) shows the**

159   **structures of the five proteins simulated in this study. Panel (B) shows the structure**

160   **of PMB1 and panel (C) provides a summary of SASA versus time for each system.**

161

7

162   The dynamics of water was also impacted by crowding (Fig. 2B), with a D_t rate of 4.93 ±

163   0.4 x 10^{-5} cm^2/s in PMB_{only} compared to 2.49 ± 0.1 x 10^{-5} cm^2/s in PMB_{crowd} for the 50-100

164   ns time period. The values found for systems in the presence of the outer membrane are

165   similar to a previous report[32] of simulations of the outer membrane in water using the SPC

166   water model[33] and with crowded simulations[34] using a different water model. Protein

167   diffusion rates were also calculated for the PMB_{dil}, PMB_{prot}, and PMB_{crowd} systems,

168   showing D_t values that also decrease with increasing crowding volume fraction ϕ.

169   Although LolA is neither bound to the cell wall nor anchored/embedded in the membrane,

170   its calculated D_t falls in the same range as the other proteins indicating that overall protein

171   motion is quite restricted in the crowded systems for all proteins. While the environment

172   we have simulated is more complex due to the presence of membrane and cell wall, the

173   diffusion rates for proteins calculated here are comparable to previous reports involving

174   simulations of crowded environments[35] and cytoplasm models[36,37], as well as with

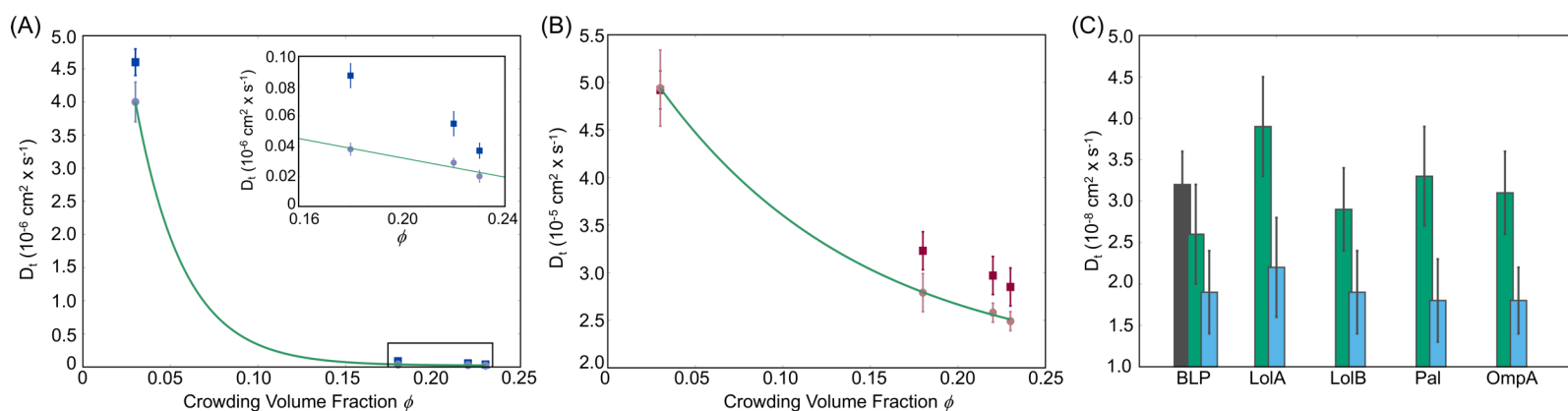175   experimental data from GFP proteins at the periplasm and cytoplasm[38].

176

178   **Figure 2**: **Translational diffusion coefficients (D_t) obtained for PMB1 (left panel),**

179   **water (middle panel), and proteins (right panel). (A): Dt values calculated for two**

180   **different time regimes, 1-10 ns (blue) and 10-100 ns (grey), as a function of the**

181   **crowding volume fraction ϕ of each system (PMB_{only} = 0.03; PMB_{dil} = 0.18; PMB_{prot}**

182   **= 0.22; PMB_{crowd} = 0.23). (B): D_t values obtained for water molecules in the same**

183   **time regimes as above, 1-10 ns (red) and 10-100 ns (pink), as a function of the**

184   **crowding volume fraction ϕ. Exponential fits were applied for the long-time scale**

185   **regimes. (C)*: Histogram showing D_t values for each protein in each system (PMB_{dil}***

186   **= black; PMB$_{prot}$ = green; PMB$_{crowd}$ = blue). Error bars indicate standard error for all**

187   **molecules across all repeat simulations.**

188

189   In this study we seek to characterize the molecular interactions that underpin the

190   aforementioned SASA, lateral motion and translational diffusion profiles calculated from

191   our simulations. The complexity of the system composition is such that a vast amount of

192   data regarding molecular interactions is generated from these simulations. To facilitate

193   interpretation of the observations we have presented the results from the perspective of

194   PMB1 interactions, namely PMB1 interactions with itself, osmolytes, proteins, and the cell

195   wall.

196

197

198   **PMB1 self-interactions**

199

200   In systems containing only PMB1 in solution (PMB$_{only}$), differently sized aggregates

201   (dimers to pentamers) formed during the simulations. The lifetimes of interactions

202   between PMB1 molecules ranged from short periods (a few nanoseconds) to longer term

203   interactions (200-400 ns) leading to formation of aggregates, as shown in the example in

204   Fig. 3A-B. A range of different configurations were observed during the simulations. The

205   majority of the interactions occurred *via* the hydrophobic portions of PMB1, namely Lip1,

206   DPhe7, and Leu8, while the charged sites remained largely exposed to water and ions

207   (Fig. 3A-B). In the example of a tetrameric association as shown in Fig. 3A, four of the

208   PMB1 molecules had their Lip1 tails buried in the middle of the aggregate along with two

209   DPhe7 and three Leu8 moieties, thus forming a structure that resembled a micelle. Due

210   to the exposure to the aqueous environment of the positive charges and polar residues

211   in this tetramer, the surface of the micelle-like structure was decorated by Cl$^-$ ions, which

212   interacted mostly with the NH$_3^+$ groups from Dab residues. The center of the micelle was

213   mostly protected from exposure to water (Fig. 3D), with only one constant water molecule

214   present at 0.5 nm (Fig. S3). This self-assembly behavior has previously been reported for

215   other similar amphiphilic antibiotics, such as colistin and colistin methanesulfonate

216   (CMS), but shown not to occur for the non-amphiphilic polymyxin B nonapeptide, an

217   analogue that lacks the hydrophobic tail[39]. In the cases previously reported, aggregate

9

218   diameters were calculated to have a z-average of around 2 nm ± 0.3, which correlates

219   well with the tetrameric aggregate observed in our simulations (2.2 nm ± 0.5). Thus, as

220   predicted for colistin and its analogue[39], PMB1 micelle formation followed a "closed

221   association" model, where the number of monomers per micelle does not exceed five in

222   our simulations. In the PMB_{dil}, PMB_{prot}, and PMB_{crowd} systems, interactions between

223   PMB1s resulted in smaller aggregates, generally involving dimerization (but with the

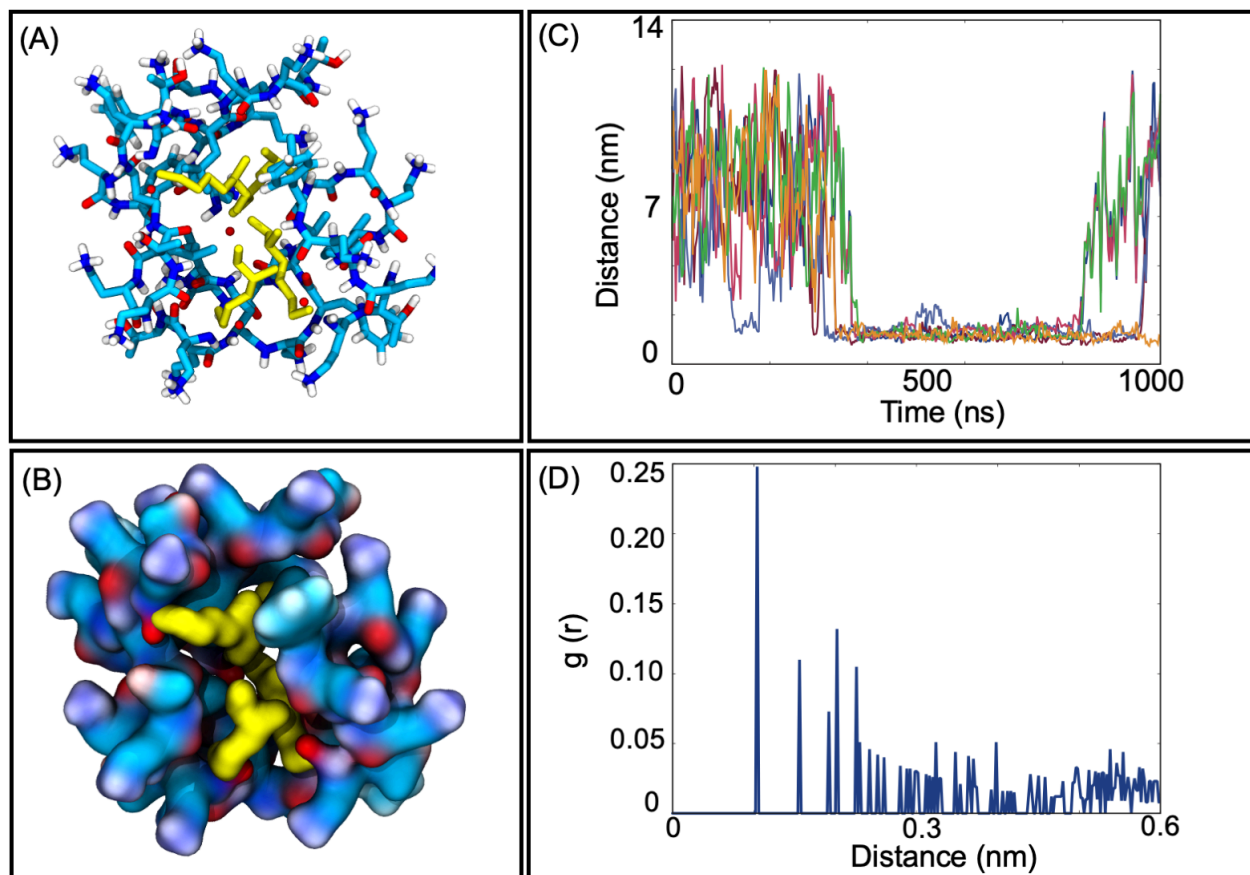224   additional participation of other molecular species, as discussed in the next section).

225

226   **Figure 3: Micelle-like associations observed during the simulations. Sticks (A) and**

227   **surface (B) representations of a tetrameric micelle, with the hydrophobic portions**

228   **pointing inwards the aggregate colored in yellow. (C) Distances calculated between**

229   **the center of mass (COM) of each monomer composing the micelle structure. Each**

230   **curve describes the distance between two different monomers, with values below**

231   **the 2 nm threshold indicating an association. (D) Radial Distribution Function**

232   **(RDF) for water molecules calculated using the COM of the whole aggregate as a**

233   **reference point.**

10

234

PMB1 interaction with osmolytes

236   The interaction of PMB1 with osmolytes and ions was firstly characterized by measuring

237   the proximity of each type of osmolyte to PMB1 molecules. The radial distribution function

238   (RDF) of each osmolyte with PMB1s as a reference (Fig. 4) showed a clear preference

239   for glycerol and OPG. This is reasonable considering the number of polar groups

240   available for interactions on both osmolytes and the negative charge (-1 e) on the

241   phosphate group of OPGs. Putrescine, spermidine and Na$^+$ ions were found furthest from

242   PMB1, which correlates with both being positively charged (putrescine = +2 e, spermidine
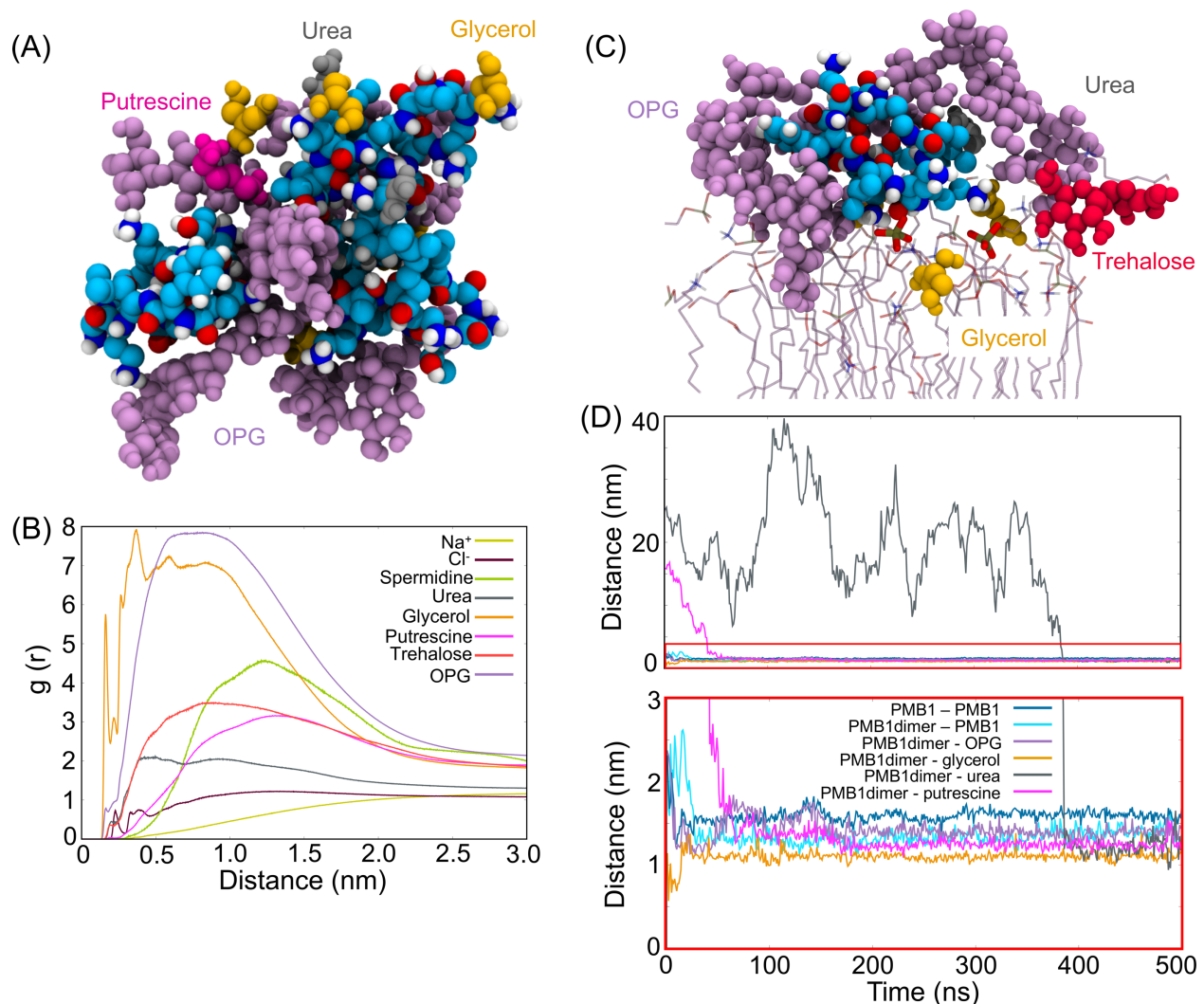
243   = +4 e).

244

11

Figure 4: Osmolyte distribution and cluster formation in PMB$_{crowd}$. (A) Cluster formed by three PMB1 molecules (cyan, white, red, blue), five OPG molecules (violet), four glycerol molecules (orange), two urea molecules (grey) and one putrescine molecule (magenta). (B) Radial distribution function (RDF) using PMB1 as a reference point with Glycerol (orange), OPG (violet) and Cl$^-$ (maroon), Na$^+$ (yellow), Putrescine (magenta) and Spermidine (light green), urea (grey) and trehalose (red). (C) Cluster formed at the surface of the outer membrane involving one PMB1 molecule, three OPG molecule, two glycerol molecules, one urea molecule and one trehalose molecule (colors as in (A)). Phosphate groups (brown and red sticks) form salt bridge interactions with Dab6 and Dab10 residues of PMB1. (D) Distances between representative molecules forming clusters are shown in panel (A), with a zoomed-in area marked with a red rectangle. Colored curves correspond to PMB1-PMB1, PMB1dimer-PMB1, PMB1dimer-OPG, PMB1dimer-glycerol and PMB1dimer-urea.

It has been discussed previously[35,40-44] that in crowded cellular environments, non-specific binding occurs constantly, generating transient clusters that affect the structure and dynamics of the molecules in this environment. In the simulations performed here, we observed formation of small osmolyte-PMB1 clusters which had an average size ~2.5 - 3.0 nm (slightly larger than the PMB1 micelles described in the previous section). These clusters generally contained PMB1 monomers interacting directly with OPG (*via* -OH groups and cyclohexane rings) and glycerol (*via* -OH groups), although participation of other osmolytes such as putrescine and urea was also observed, but usually without these molecules directly interacting with PMB1. In particular, the association between PMB1 molecules and OPG was prevalent (as shown in the RDF in Fig 4). For example, in one case, four OPG molecules bound around the surface of a PMB1 dimer (Fig. 4A), while a fifth OPG molecule mediated the interaction between the PMB1 dimer and a third PMB1 molecule. Four additional molecules of glycerol, one putrescine and two urea molecules also participated in this cluster, effectively bridging the PMB1 dimer to the third PMB1 (Fig. 4D), stabilizing the complex. This cluster took ~ 100 ns to stabilize in terms of number of components, apart from one urea molecule which only joined the cluster

276   after 400 ns (Fig. 4D and 4E). The final cluster shape was achieved at around 420 ns and

277   remained stable until the end of the simulation. The largest cluster in all simulations was

278   ~ 4.2 nm in diameter and was composed of four PMB1 molecules and ~20 osmolytes

279   (one trehalose, five putrescine, seven glycerol and seven OPG). In this cluster, only two

280   of the PMB1 molecules are directly associated with each other, interacting *via* their DPhe7

281   residues. The formation of the cluster was initiated by many of the molecules binding to

282   the cell wall (within 30 ns of the start of the simulation), while the full cluster had formed

283   after ~100 ns and lasted for around 240 ns. Despite showing a higher preference for

284   cluster formation in the cell wall area, a few aggregates were also observed on the surface

285   of the inner leaflet of the outer membrane (Figure 4C). For example, in one cluster, one

286   PMB1 molecule is surrounded by three OPG molecules, two glycerol molecules, one

287   trehalose molecule and one urea molecule. Glycerol not only intermediates interactions

288   between PMB1 and OPG, but also with 1-palmitoyl,2-cis-vaccenyl-phosphatidyl

289   ethanolamine (PVPE) lipids, in this aggregate. PMB1 also interacts with PVPE *via* Dab6

290   and Dab10 - phosphate salt bridges. Additionally, the cluster was visited by two

291   putrescine molecules – one remaining in the aggregate for 160 ns and the other for only

292   50 ns.

293

PMB1 interaction with proteins

295   The number of interactions between PMB1 molecules and proteins were calculated based

296   on intermolecular contacts (distances < 0.4 nm) during the course of the simulations,

297   values concatenated over all trajectories for each protein are provided in Table S1.

298   Interactions of PMB1 were observed with all of the different proteins in the systems. We

299   consider the lipoprotein carriers, LolA and LolB first. In PMB_{prot} and PMB_{crowd} PMB1

300   molecules were found interacting both near to and at the entrance to the hydrophobic

301   cavities of both proteins (Fig. 5 and 6). It is a useful reminder here that the normal function

302   of LolA and LolB requires the lipid tails of cargo lipoproteins to bind in their hydrophobic

303   cavities. A number of different PMB1 to LolA/B binding events were observed in our

304   simulations. For example, in the PMB_{prot} system three molecules of PMB1 were observed

305   to interact with the entrance to the cavity of LolA simultaneously (Fig. 5A), throughout one

306   of the 500 ns simulations, with one partially inserted into the cavity. The LolA residues

13

307 involved in theses interactions range from hydrophobic to charged: Trp49 (51%), Met51

308 (95%), Thr52 (69%), Gln53 (72%), Pro54 (46%), Asp55 (45%), Phe72 (32%) and Glu74

309 (25%), where parentheses indicate percentage of simulation time for which the

310 interactions existed, reflecting the chemical diversity of PMB1. Interestingly, in PMB_{prot},

311 one molecule of PMB1 bound to the entrance of the LolB cavity with its Lip1 residue

312 inserted into the cavity (Fig. 6). Due to the extended conformation adopted by this PMB1,

313 several LolB residues participated in long-lasting interactions (more than 60% of total

314 simulation time) (Fig. 6B-C) with PMB1, including residues previously predicted as

315 important for the binding of acyl chains[45], namely Phe37, Val46, Met107 and Ile109. This

316 indicates that PMB1 can bind in the LolB cavity in a manner that resembles normal the

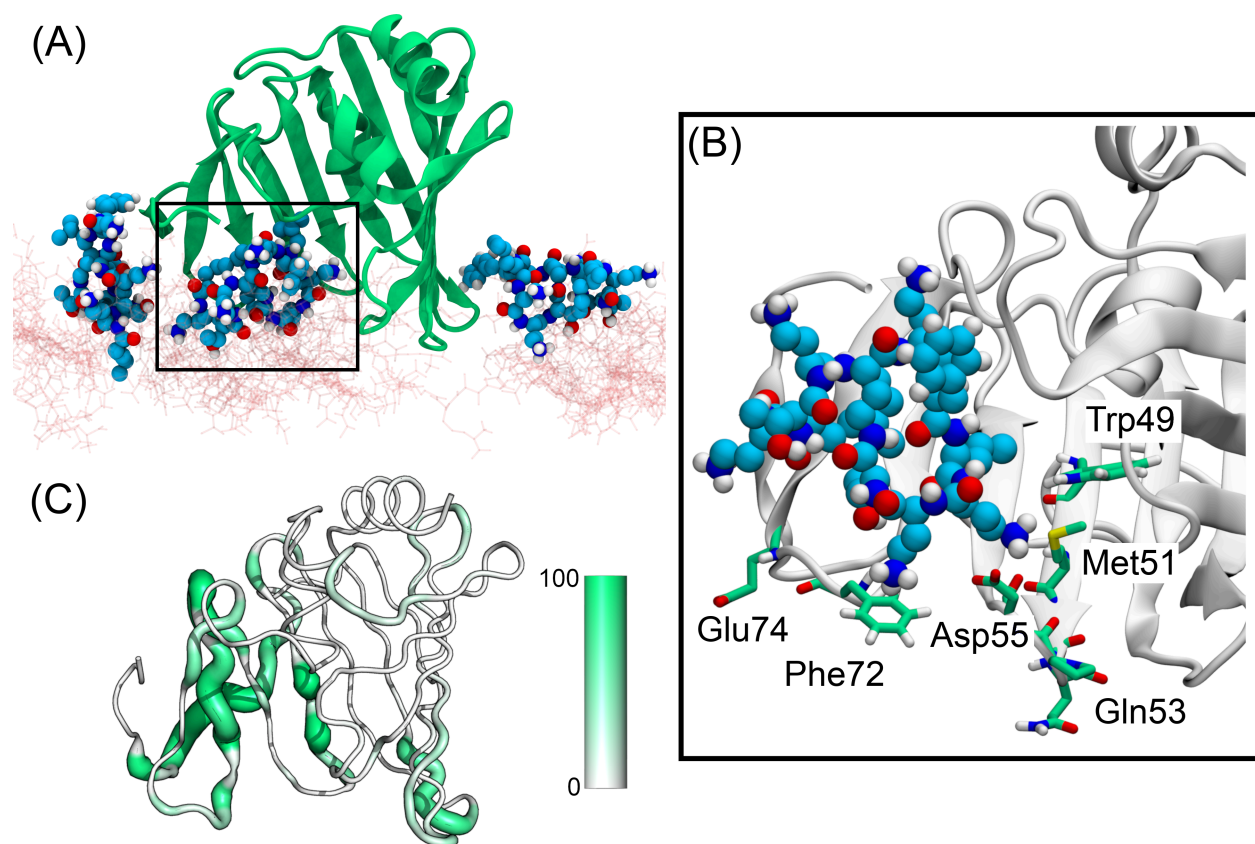317 binding of acyl chains of lipoproteins to LolB.

318

319

320 **Figure 5: PMB1 binding modes to LolA. In PMB_{prot}, three PMB1 bind to LolA at the**

321 **same time (A) LolA = green, PMB1 = as previously, cell wall = pink sticks). One**

322 **PMB1 is partially inside the hydrophobic cavity. (B) Zoomed in region where PMB1**

323 **is bound to the hydrophobic cavity of LolA, interacting mainly with residues Trp49,**

14

324 **Met51, Gln53, Asp55, Phe72, and Glu74. (C) Sausage representation of LolA with**

325 **respect to PMB1 interactions. Regions of the protein with higher percentage of time**

326 **spent interacting with PMB1 are shown as enlarged tube, while regions with fewer**

327 **interactions are shown as narrower tubes.**

328

329 Next we consider PMB1 - Pal interactions. In both the PMB1$_{crowd}$ and PMB1$_{prot}$

330 simulations, PMB1 was observed sandwiched in between the C-terminal domain (CTD)

331 of Pal, the linker domain and the outer membrane. The interactions lasted for the entirety

332 of the simulations. Pal residues involved in the interactions are provided in Table S1.

333 Furthermore, upon PMB1 binding, the motion of the linker region of Pal become more

334 restricted (Fig. S4), but the initial non-covalent interaction of Pal with peptidoglycan

335 seems to be unaffected (Fig. S5). Despite that, this binding to the linker appears to limit

336 the increase in number of contacts between Pal and the cell wall, when compared to

337 systems that do not have a PMB1 attached to the linker (Fig. S5). More transient PMB1-

338 Pal binding events also occurred in simulations of each system. In PMB$_{prot}$, a PMB1

339 molecule entered the area in between the cell wall and the CTD of Pal (residues Ala109,

340 Asp110, Arg112, Thr114, Tyr117 and Gly149), after initially being bound to a BLP for 370

341 ns (Fig. S6A). Other examples of PMB1 exchanging binding partners were also observed

342 from Pal to LolA (Fig. S6B), from BLP to LolB (Fig. S6C), and from BLP to BLP (Fig. S6D).

343 Thus, showing that within 500 ns PMB1 can move from interacting with one protein to

344 another. In PMB$_{crowd}$, after intermittently interacting with Leu176 and Lys185 in the Pal

345 CTD for 160 ns, one PMB1 moved slightly away from Pal and associated with another

346 PMB1 forming a dimer (Fig. S7). While the same region of Pal that was previously bound

347 to the original PMB1 formed an interaction with a small cluster containing one molecule

348 of OPG, one molecule of Glycerol and one molecule of putrescine. This small cluster also

349 simultaneously interacted with the newly formed PMB1 dimer, which at this stage was not

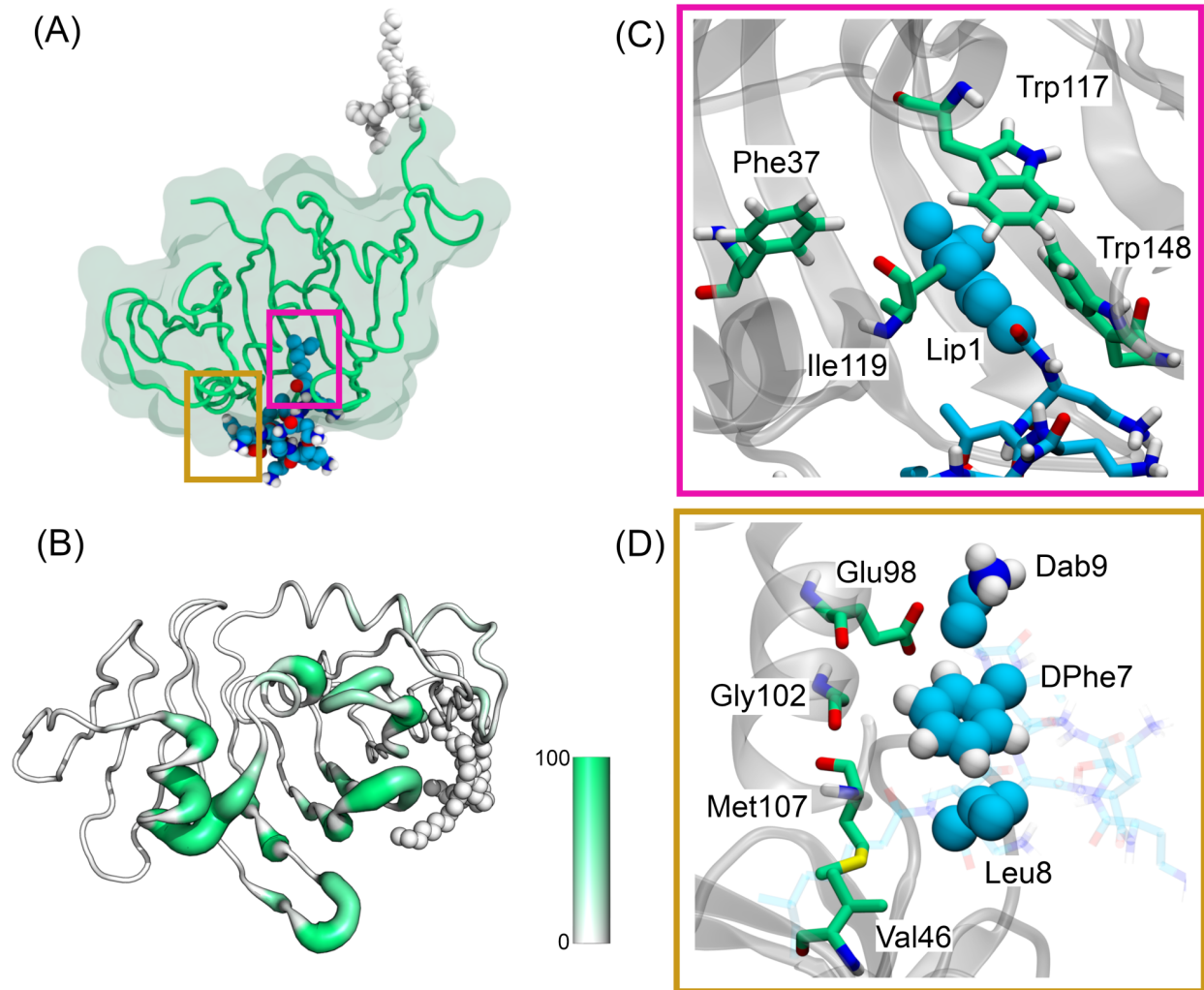350 directly interacting with Pal.

15

351

Figure 6: PMB1 binding mode to LolB. (A) PMB1 inserts Lip1 inside the hydrophobic cavity of LolB, reaching hydrophobic residues that usually interacts with acyl chains from lipoprotein ligands. (B) Sausage plot representation of the structure of LolB. Regions of the protein with higher percentage of time (from 0 to 1, coloured from white to green) spent interacting with PMB1 are shown as enlarged tube, while regions with less interactions are shown in thinner tubes. (C) Zoomed-in region showing binding at the hydrophobic cavity of LolB. In this area, Lip1 interacted with Phe37, Ile109, Trp117, and Trp148. (D) Zoomed-in region showing binding at the exterior part of LolB. In this region DPhe7, Leu8 and Dab9 interacted with residues Val46, Glu98, Gly102 and Met107.

362

363   PMB1 interactions with OmpA were mainly with the CTD. Each system had two or three

364   PMB1 molecules binding to OmpA simultaneously. At least one molecule in each system

365   was bound at the interface between the OmpA CTD and the cell wall, mediating the

366   interaction between both structures. This binding region was located between the two

367   main helices (composed of residues Glu212 to Asn226 and Ser253 to Lys267) from the

368   CTD, with a prominent role of residues Gln214 (92%) and Tyr263 (87%). Interactions

369   were hydrogen-bonding (Dab9 - Gln214) and hydrophobic (DPhe7 and Leu8 – Tyr263) in

370   nature. Pal and OmpA have some structural similarities in their C-terminal domains

371   (similarity of 35%), and both are known to bind to the cell wall[46-48]. Analysis of the contact

372   data between PMB1-Pal and PMB1-OmpA revealed two long-lived interactions involving

373   a specific helix from the CTD of each protein. This helix is composed of residues

374   H_{112}ANFLRSNPS$_{122}$ in Pal and Y$_{244}$SQLSNLDP252 in OmpA. Interestingly this region

375   forms part of the dimerization interface of OmpA, thus would only be available for

376   interaction when the protein is in its monomeric state[16,48]. Additionally, PMB1 was

377   observed to bind to these regions while simultaneously interacting with adjacent motifs

378   (Fig. S8) in both proteins: Q$_{63}$MQQLQ$_{68}$ in Pal (a short helix) and K$_{290}$GIPADKIS$_{298}$ (a

379   loop connecting an α-helix to a β-strand). Interestingly only one PMB1 across all

380   simulations was observed binding directly to the linker region of OmpA (in PMB$_{prot}$), in

381   PMB$_{crowd}$, the linker area is largely occupied by osmolytes.

382   Comparison of data from PMB1 binding to BLP and Pal, revealed a short motif comprising

383   the sequence S-S-E/D/N-X-Q/N (Fig. S9). Serine and acidic residues have particular

384   propensity to interact with PMB1 (Fig. S10) due to the possibility of interacting *via*

385   hydrogen bonding or salt bridges. Interactions between these residues are PMB1 lasted

386   from 20 ns up to 400 ns. In simulations containing proteins, the four BLPs were the main

387   target of binding events, with an average of 6 molecules of PMB1 binding to the four BLPs

388   per system simulated. Regions of longest interactions (over 70% of simulation time)

389   include residues S$_{11}$SDVQTLNA$_{19}$ (at the vicinity of the cell wall) and Asp34, Asp41,

390   Ala42, Ala43, Arg48 (adjacent to the outer membrane). A number of the molecules

391   interacting with BLP were also inserted in the interface with either the cell wall or the outer

392   membrane in all of the simulations. Interestingly, in the PMB$_{crowd}$ system most of the

393   PMB1s that interacted with BLP were located in the solution region. The interfacial

17

394 regions favoured by PMB1 in other systems (PMB$_{dil}$ and PMB$_{prot}$) were occupied by

395 osmolytes in PMB$_{crowd}$. Thus, the presence of osmolytes seems to force PMB1 into the

396 solution to some extent, by occupying interfacial binding regions.

397

PMB1 interactions with the cell wall

399 A number of PMB1 molecules (at least 14) reached the peptidoglycan layer area very

400 rapidly (within the first 10 ns) in all simulations (Fig. S1 and S11). The negative charges

401 presented by D-Glu and meso-diaminopimelate (m-DAP) residues from the peptide

402 portion of the cell wall interact with PMB1. Other interactions are also present, such as

403 PMB1 forming hydrogen bonds to the hydroxyl groups attached to the pyranosidic rings

404 of the peptidoglycan glycan strands (Fig. S12). None of the PMB1 molecules were

405 observed to go through the pores of the cell wall and dissociate from it during the total

406 time of 3 μs of all simulated systems. Most osmolytes also did not cross through the pores

407 easily: only putrescine, trehalose and urea were able to cross multiple times (Fig. S13).

408 Generally, two modes of association between PMB1 and the cell wall were observed. In

409 one mode, PMB1 inserts itself between glycan strands, as seen in one example from

410 PMB$_{dil}$ system (Fig. 7A). In some cases, it acted similarly to a peptide linkage, as it was

411 able to form salt bridge interactions with both glycan strands simultaneously for more than

412 200 ns (Fig. 7C), decreasing the local distance between the strands from ~2.7 nm to ~1.9

413 nm. The other observed mode of association is PMB1 attaching to the surface of the cell

414 wall, not inserted between the strands, but rather located around peptide linkages (Fig.

415 7B). A common aspect from both binding modes is that the Dab residues from PMB1

416 attract the loose peptide portions (not connected to > 1 glycan strand), forming salt

417 bridges. The insertion mode of interaction involved the formation of multiple long-lived (~

418 200 ns) salt bridges with the Dab - m-DAP and Dab - D-Glu, in contrast, in the surface

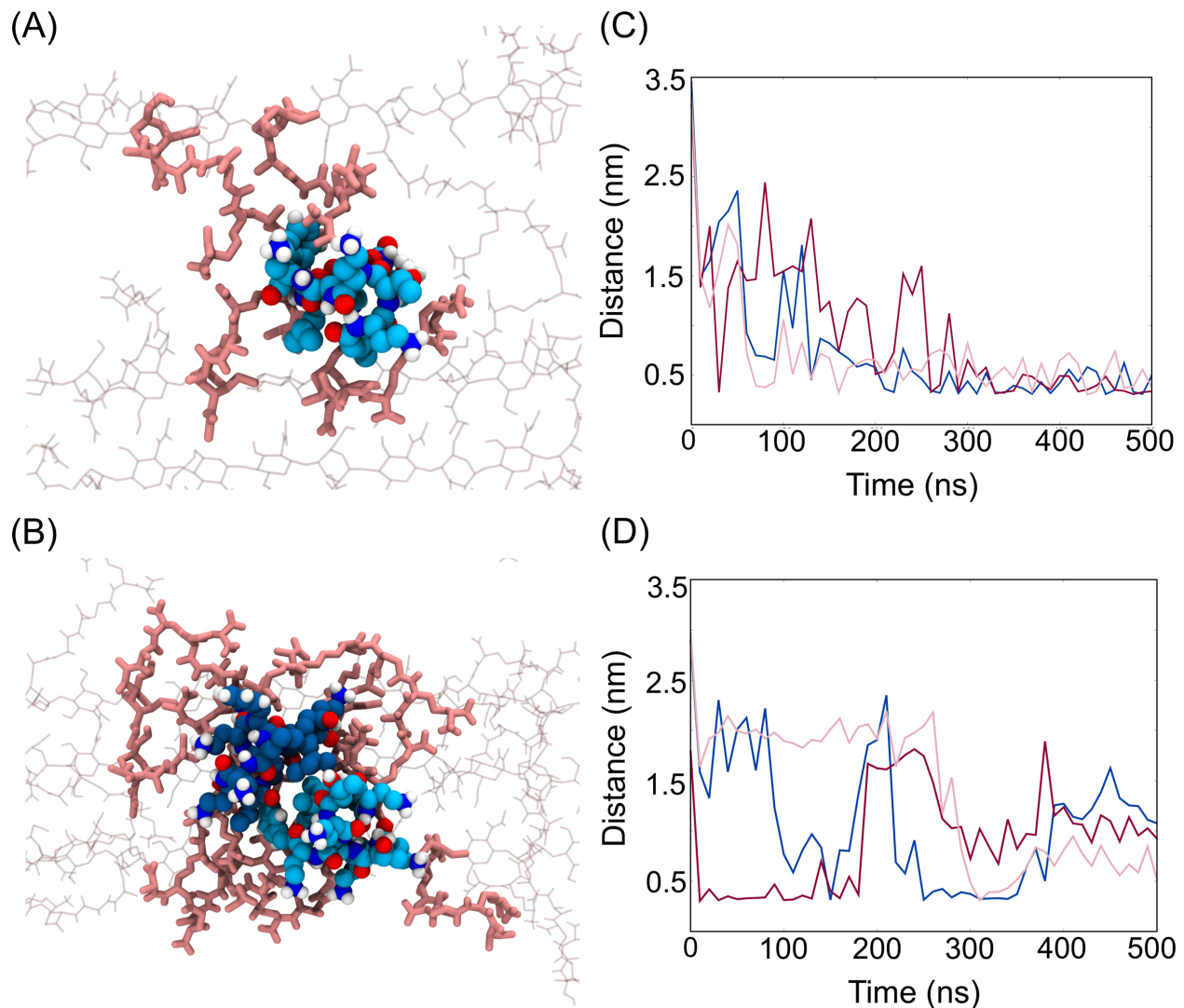419 binding mode the salt bridges had a lifetime of ~ 100 ns. (Fig. 7D).

18

Figure 7: PMB1 binding modes to the cell wall extracted from PMB$_{dil}$ and PMB$_{prot}$. **The inserted binding mode is depicted on (A), showing PMB1 (blue carbon spheres) attached inside of the pores of the cell wall (pink sticks) and interacting with many negatively charged residues. The surface binding mode is depicted in (B), showing a PMB1 dimer (two shades of blue) bound to the surface of three glycan strands. (C) and (D) shows examples of distances of salt bridges interactions between different Dab residues (PMB1) and m-DAP and D-Glu (cell wall). In the inserted binding mode, interactions seem to last longer overall than in the surface binding mode.**

19

432   In the PMB$_{prot}$ system, a few of the PMB1 molecules mediated protein binding to the cell

433   wall (Fig. 8). For example, PMB1 bound to the surface of LolA, interacting with residues

434   Lys23, Asp26 and Glu34, while at the same time interacting with m-DAP and D-Glu from

435   the cell wall. An observation from both simulations of the PMB$_{prot}$ system, was an

436   extension of the OmpA linker region that appeared to be induced by PMB1 which is bound

437   to the CTD region. By around 420 ns, there is an increase in the number of residues from

438   OmpA contacting the cell wall, increasing from 5 to 10 (Fig. S14). This appeared to occur

439   spontaneously, but subsequently the PMB1 Dab residues form salt bridges with three

440   charged groups (two D-Glu and one m-DAP) of the loose peptide ends of the cell wall

441   (Fig. 8 and S14). These interactions of PMB1 which is bound to both OmpA and the cell

442   wall, seemed to have acted as a driving force to push the OmpA CTD further towards the

443   cell wall, stabilizing and increasing the OmpA-peptidoglycan binding interface from 10

444   residues to almost 20. Similarly, in the PMB$_{crowd}$ system, some associations between the

445   PMB1, proteins (OmpA, LolA and Pal) and the cell wall were also observed. For example,

446   initially, a PMB1 is associated with the OmpA CTD mediated by two trehalose molecules

447   and one glycerol molecule (Fig. 8). At the same time, the same PMB1, one of the

448   trehalose, glycerol and residue Asn249 of OmpA were in the vicinity of the cell wall (within

449   0.6 nm), displaying a few hydrogen bonding interactions. By the end of the simulation,

450   this cluster had dissociated. Another example is the PMB1-Pal association mentioned in

451   the previous section with the presence of a small cluster of osmolytes (Fig. 8). Residue

452   Asp179 of Pal interacted with OPG, glycerol, and putrescine molecules while they were

453   bound to PMB1 and/or the cell wall, the interaction partners in this cluster changed

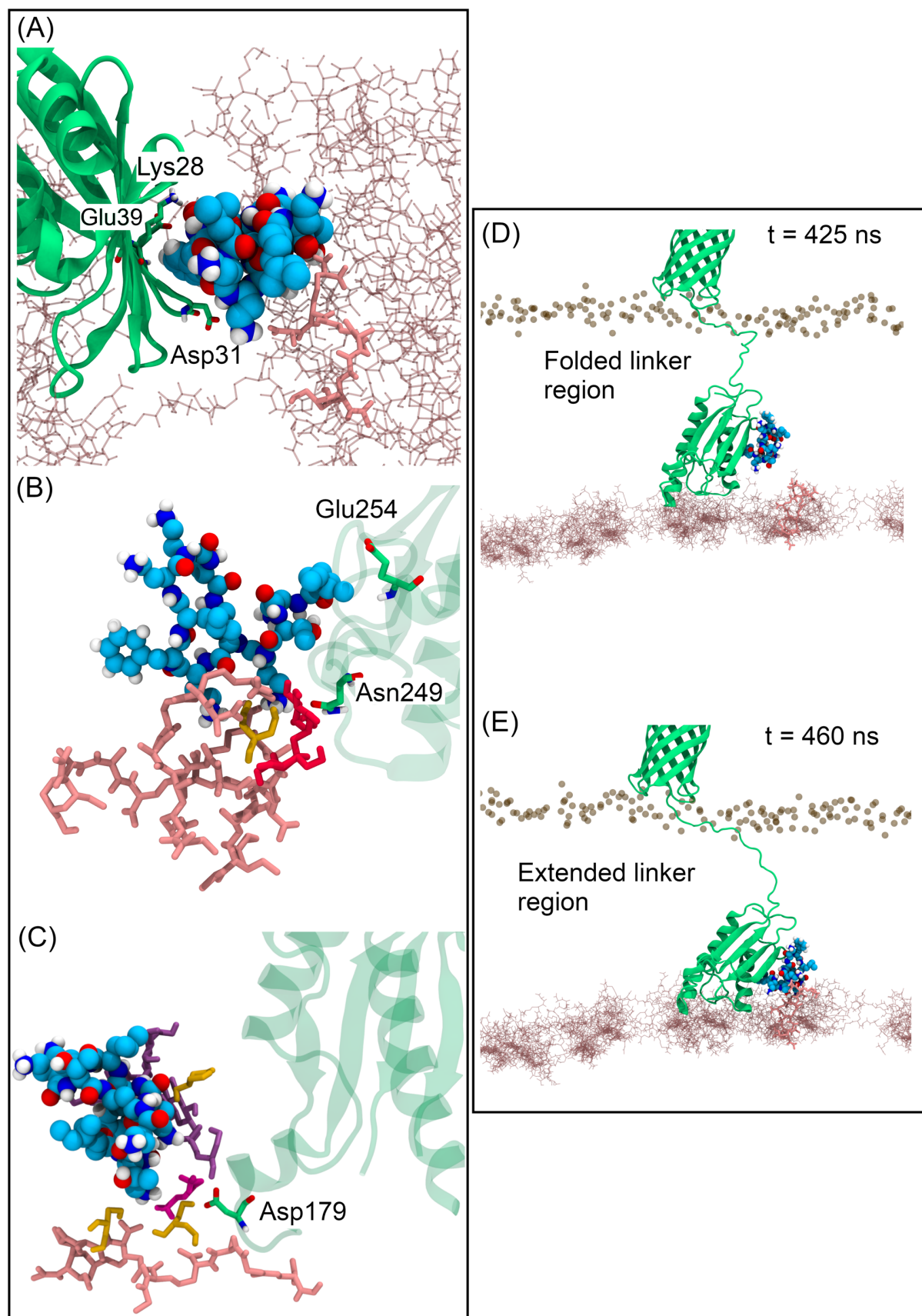454   frequently over time, indicating the non-specificity of these intermolecular associations.

455

21

456 **Figure 8: PMB1 mediating interactions between LolA, Pal, OmpA (green) and the**
457 **cell wall (pink sticks). Panel (A) shows highlighted residues Asp26, Lys23 and**
458 **Glu34 (green) from LolA interacting with Dab (Asp26) and DPhe7 (Lys23 and**
459 **Glu34,) from PMB1 (colored in blue spheres), while another Dab from PMB1**
460 **interacts with a negative charged residue from the cell wall (pink licorice sticks). In**
461 **Panel (B), PMB1 and osmolytes (glycerol – orange; trehalose – red) are shown**
462 **mediating interactions for OmpA-cell wall. In (C), a bigger cluster containing OPG,**
463 **putrescine, glycerol and urea is shown mediating interactions with Pal and the cell**
464 **wall. Panels (D) and (E) depict two different states of OmpA and PMB1, before (D)**
465 **and after (E) enhancing the interaction with the cell wall. In (B) and (C), only cell**
466 **wall residues that are in contact with PMB1 and osmolytes are shown to improve**
467 **clarity.**

468

469 # Discussion

470 Currently there is a great need to find novel therapeutic agents to address the problem of
471 antimicrobial resistance to antibiotics[49,50]. In order to do so in a rational manner requires
472 a thorough understanding of the environment faced by antibiotics such as PMB1 as they
473 negotiate the bacterial cell envelope. In this work, we have simulated an atomistic model
474 of the periplasmic space to study the fate of PMB1 in this region once it has already
475 crossed the OM. Our results predict that PMB1, and likely other drugs relying on diffusion
476 alone to cross the periplasm, face a complex path, full of molecular obstacles which hinder
477 their movement through the periplasm. The presence of structures from subcellular
478 compartments in our model systems had a major effect on the diffusion coefficients of
479 PMB1 molecules. This was observed by the 100-fold reduction in values in the periplasm
480 models compared to PMB1 just in solution. Similarly, diffusion of native proteins was also
481 affected by increased crowding. Previous studies of diffusion rates in the cytoplasm and
482 the periplasm showed that the GFP proteins have a slightly slower diffusion rate in the
483 periplasm[38] when compared to the cytoplasm and there have been some discussions in
484 the literature regarding the nature of the periplasm being a gel-like environment[51] or a
485 fluid environment[38]. At the level of crowding we have in our simulations the system is
486 clearly still fluid. Crowding up to 30% of volume has been reported previously to have

487   modest effects on water properties[34], showing alterations in the self-diffusion coefficient

488   of water that are in-line with our simulations (~20% Volume with ~2.0 x 10^{-5} cm^2/s).

489   PMB1 is an amphipathic molecule with considerable conformational flexibility. In just

490   water and ions, we observed PMB1 tetramers forming micelles with sizes comparable to

491   experimental data[30] for micelle formation in solution of colistin (polymyxin E). In addition,

492   as predicted for colistin and its analogue[39], our micelle formation followed a "closed

493   association" model, in which the number of monomers is discrete, limiting micelles to a

494   certain size (pentamers with 2.6 nm). Thus, our model of PMB1 in water provided a

495   'baseline' reference system which gave aggregate sizes and dynamical behavior that

496   reproduced experimental observables for similar molecules.

497   We observed a wide range of associations of PMB1 with other molecules. One particularly

498   interesting phenomenon observed here is PMB1 insertion into the hydrophobic cavities

499   of the lipoprotein carriers LolA and LolB. These cavities have previously been shown to

500   be non-specific binders of hydrophobic molecules[52-54]. Our results suggest it is possible

501   that some PMB1s may be carried through the cell wall by hijacking the lipoprotein carrying

502   functionalities of LolA/LolB. Given we observe PMB1 adhering to the cell wall this

503   'hitchhiking' mechanism would be advantageous in providing an easier route through the

504   cell wall. To our knowledge this spontaneous phenomenon is described here for the first

505   time. It is important to consider here other potential consequences of PMB1 binding to

506   the lipoprotein carriers. LolA and LolB play important roles in avoiding toxicity due to

507   accumulation of BLP in the inner membrane[55,56]. Binding of PMB1 into their hydrophobic

508   cavities may serve to inhibit their natural functions and lead to mislocalization of

509   lipoproteins in the inner membrane, in a similar manner to small hydrophobic inhibitors

510   such as MAC13243[52-54]. Interestingly, LolA transcription is triggered with increasing

511   concentrations of PMB, a mechanism connected to the activation of the stress regulator

512   Rcs phosphorelay system[57] which provides indirect evidence to support our hypothesis.

513   Osmolyte - PMB1 interactions varied depending upon the chemistry of the osmolyte. We

514   observed fast formation of small clusters of molecules, with PMB1 usually binding to, and

515   often becoming partially coated with the polar OPG and glycerol molecules. The OPG

516   concentration becomes slowly diluted when bacteria are moved to concentrated media[58].

517   Given the high propensity for these molecules to bind to PMB1 in our simulations, we

23

518   suggest that the changes in the OPG concentration may also impact on dynamics of

519   PMB1 in the periplasm. As discussed in previous simulation studies[34,35,37], molecular

520   crowders can promote a range of effects, including excluded volume effects and replacing

521   interactions. In our simulations, osmolytes mediate interactions between other molecules

522   and also replace some interactions. For example in the absence of osmolytes, there is a

523   greater propensity for PMB1-BLP interactions to occur at the BLP/cell wall and BLP/OM

524   interfaces, however these regions are occupied by osmolytes in the most crowded

525   system, and consequently PMB1 interactions with BLP are largely with the region of the

526   protein in 'bulk' solution in the periplasm. This suggests that the non-specific binding of

527   osmolytes to cell envelope components may have local consequences for available

528   binding modes for antibiotics.

529   Two main peptidoglycan binding modes were observed; one in which PMB1 inserts

530   in between glycan strands acting as a pseudo cross-link and one in which it is surface-

531   bound close to the peptide linkages. Atomic Force Microscopy (AFM)[59] studies have

532   suggested that the cell wall interactions formed by colistin may be responsible for

533   rigidifying the cell envelope.

534   A limitation of our results involves the correction of the diffusion coefficients for

535   finite-size effects. Given the complexity of our models, with the presence of the outer

536   membrane and the cell wall, that our simulation boxes are non-cubic, and that the

537   correction becomes smaller with increasing box size, we opted for not applying it in these

538   D_t values. Our results for proteins and water diffusion correlate well with previous

539   atomistic crowding models[34-37]. Experimental studies[38,60] reported D_t rates for GFP that

540   are in a similar range to ours. We note here that experimental value for the OmpA N-

541   terminal domain (transmembrane) alone, $D_{exp} = 4.9 \pm 0.09 \times 10^{-7}$ cm^2/s is faster than the

542   value obtained for the complete protein from our simulations ($D_t = 3.1 \pm 0.6 \times 10^{-8}$

543   cm^2/s in PMB$_{prot}$ and $D_t = 1.8 \pm 0.5 \times 10^{-8}$ cm^2/s in PMB$_{crowd}$). The C-terminal domain of

544   OmpA is bound to the peptidoglycan which is highly likely to be the cause of the slower

545   diffusion in the simulations.

546   It is also worth mentioning that the SPC water model (which works well with the

547   GROMOS54a7 force field[61]) overestimates experimental values of self-diffusion for water

548   molecules[62], so D_t values for solutes possibly are affected by this. Finally, crowding

24

549 systems simulations are very complex and could lead to intense aggregation when using

550 standard additive force fields[63,64], with several methods being proposed to solve this[65,66].

551 From our perspective, GROMOS54a7 was a reasonable choice, since it is one of the

552 force fields that shows a lesser preference for the aggregated state[70], while also having

553 validated parameters for the complex mixture of lipids that compose the bacterial outer

554 membrane and the bacterial cell wall. Our results where comparable with other

555 experimental and simulation studies are in-line with those, providing further confidence in

556 the predictions from the complex simulations which go beyond previous studies in terms

557 of the resolution and complexity of the simulations studied.

558

559 Conclusions

560 In conclusion, atomistic molecular dynamics simulations of the antibiotic PMB1 in a

561 number of models of the periplasm of Gram-negative bacteria with differing levels of

562 crowding have revealed slower diffusion of the antibiotic as the periplasm becomes more

563 crowded. PMB1 forms complexes with osmolytes, the cell wall and native cell envelope

564 proteins which can be short-lived or long-lived. PMB1 is rarely uncomplexed within the

565 periplasm, therefore its functional groups are occupied in interaction with other species

566 more often than not. We feel this is an important factor to consider in future development

567 of antibiotics (and may be extended to drugs that target other organisms too). The *in vivo*

568 environment is not a chemistry experiment in which ones controls the type and number

569 of molecules involved, and the complexity of the former may impact upon foreign

570 molecules such as drugs in many unexpected ways. The simulations described here

571 show that incorporation of the chemical details of the local environment can predict likely

572 interactions with other species and highlight potential mechanistic pathways that may

573 have been originally unintended (such as the ability of PMB1 to bind to LolA and LolB).

574

575 Methods

576

577 System Preparation

578   We constructed the template model based on previously published works from our

579   group[17,48,67]. This was composed by an asymmetric outer membrane (OM) of an identical

580   composition as seen in previous works[17,67-69], a one-layer peptidoglycan cell wall (PGN)

581   formed by 12 glycan strands of 17 repeating NAG-NAM-peptide units, four Braun

582   Lipoproteins (BLP) covalently attached to PGN and inserted in the membrane by

583   tripalmitoyl-S-glyceryl-cisteine residues[67,69]. Models for BLP(PDB: 1EQ7)[70], LolA (PDB:

584   1IWL) and LolB (PDB: 1WLM)[45], OmpA[16], Pal (PDB: 2W8B)[71] were taken from previous

585   works from the group[72,48,54,67]. Pal and OmpA proteins were also included in PMB_{prot} and

586   PMB_{crowd} systems. Crystallographic structures of LolA and LolB GROMOS 54A7 force

587   field with the GROMOS 53A6OXY ether parameters[73] were used for the construction of

588   the tripalmitoyl-S-glyceryl-cysteines. After setting up this initial template system, we

589   added the other components: Pal bound and unbound to the cell wall, PMB1 molecules,

590   and ions concentrations. PMB1 GROMOS 54a7 parameters were obtained by using the

591   Automated Topology Builder (ATB) server[74]. For OmpA insertions into the OM, we

592   employed the *gmx membed* tool[75], similarly to a previous report[67].

593   For the construction of the PMB_{crowd} system, parameters for the molecular crowders were

594   obtained using the ATB server, with the exception of OPG and trehalose, in which the

595   GROMOS 56a6 (CARBO)[76] parameters were employed, which are compatible with

596   GROMOS 54a7. We adapted the "droplet methodology" from Bortot *et al*[37] to deal with

597   the insertion of osmolytes, by adding each osmolyte with a water shell obtained from 100

598   ns molecular dynamics simulations.

599

Atomistic Molecular Dynamics Simulations

601   We performed molecular dynamics simulations employing the GROMACS simulation

602   suite (version 2018.3)[77] along with GROMOS54a7 force field[61] and SPC water model[33].

603   We divided the simulations in two parts: equilibration simulations in NVT and NPT

604   ensembles with position restraints in proteins, cell wall, and PMB1, which lasted for 1 and

605   100 ns, respectively; and production simulations in NPT ensemble, which ran for 500 ns.

606   Simulations were performed at 310 K, which was maintained by employing the velocity

607   rescale thermostat[78] with a coupling constant of $\tau = 0.1$. Pressure was maintained semi-

608   isotropically at 1 atm by employing the Parrinello-Rahman barostat[79] with a time constant

26

609 of 2 ps. The particle mesh Ewald method treated long-range electrostatics[80]. LINCS

610 algorithm[81,82] constrained the covalent bonds, which allowed an integration step of 2 fs.

611 Both long-range electrostatics and van der Waals cutoffs were set to 1.4 nm. To neutralize

612 charges, we added the correct number of counterions together with an extra salt

613 concentration of 0.2 M of sodium chloride ions for all simulations. For the replicates,

614 starting positions of the proteins and PMB1 molecules were changed, along with re-

615 solvation of the system, equilibration and production phases. In addition, we modified the

616 starting velocities to ensure the difference between runs and improve conformational

617 sampling. For molecular manipulation, visualization, and analysis, we employed the VMD

618 software[83].

619

620 **Analysis**

621 Translational diffusion coefficients, D_t, were obtained by using the *gmx msd* analysis tool

622 from the GROMACS tool set to calculate the mean square displacements (MSD). MSD

623 plots (Figure S2) were calculated for time delays The linear fit (where the slope was

624 obtained) was performed in different time regimes (1-10 ns; 50-100 ns) for PMB1 and

625 water (1-10 ns; 10-100 ns) aiming to capture the slowdown in D_t due to crowding effects,

626 while for proteins, the linear fit was performed in the range of 5-15 ns. Error estimates

627 were obtained by averaging over all and by averaging over replicate simulations of each

628 system. For the XYZ motion analysis, the *gmx trajectory* tool was employed to obtain the

629 coordinates of the center of mass of each PMB1 in the X, Y and Z axis. Radial distribution

630 function values (RDF) were obtained using the *gmx rdf* tool, while *gmx sasa* was used for

631 SASA calculations. In-house scripts were employed for the intermolecular contact

632 analysis.

633

634 **ASSOCIATED CONTENT**
635 **Supporting Information**
636
637 The Supporting Information is available free of charge on the ACS Publications website.
638
639   Further analysis of the data including Figures S1-S14 and Table S1 (PDF file).
640

641

Author Contributions

The manuscript was written through contributions of all authors. SK conceived the project, CP conducted the simulations, IPSS and AB helpeed with simulation setup and analysis, CP and SK also performed analysis, CP and SK wrote the paper. All authors have given approval to the final version of the manuscript.

647

Acknowledgements

654

References

1. Weiner JH, Li L. 2008. Proteome of the Escherichia coli envelope and technological challenges in membrane proteome analysis. Biochim Biophys Acta - Biomembr 1778:1698–1713.
2. Goemans C, Denoncin K, Collet J-FF. 2014. Folding mechanisms of periplasmic proteins. Biochim Biophys Acta - Mol Cell Res 1843:1517–1528.
3. Vaara, M. 2019. Polymyxins and Their Potential Next Generation as Therapeutic Antibiotics. Front. Microbiol. 10, 1689.
4. Morrison, D. C., Jacobs, D. M. 1976. Binding of polymyxin B to the lipid A portion of bacterial lipopolysaccharides. Immunochemistry. 13, 813-818.
5. Bader, J., Teuber, M. 1973. Action of polymyxin B on bacterial membranes, I. Binding to the O-antigenic lipopolysaccharide of Salmonella typhimurium. Z Naturforsch [C] 28, 422-430.
6. Evans, M. 1999. Polymyxin B sulfate and colistin: Old antibiotics for emerging multiresistant Gram-negative bacteria. Ann. Pharmacother. 33, 960–967.
7. Trimble, M. J., Mlynarcik, P., Kolar, M. & Hancock, R. E. W. 2016. Polymyxin: alternative mechanisms of action and resistance. Cold Spring Harb. Perspect. Med. 6, a025288.
8. Gales, A. C., Jones, R. N., Sader, H. S. 2011. Contemporary activity of colistin and polymyxin B against a worldwide collection of Gram-negative pathogens: results from the SENTRY Antimicrobial Surveillance Program (2006–09). J. Antimicrob. Chemother. 66, 2070–2074.

9. Li, Z., Cao, Y., Yi, L., Liu, J. H., Yang, Q. 2019. Emergent Polymyxin Resistance: End of an Era? Open Forum Infec. Dis. 6, ofz368.

10. Li Z & Velkov T. 2019. Polymyxins: Mode of Action. Adv. Exp. Med. Biol. 1145, 37-54.

11. Vollmer, W. & Holtje, J. V. 2004. The architecture of the murein (peptidoglycan) in gram-negative bacteria: vertical scaffold or horizontal layer(s)? J Bacteriol. 186, 5978–5987.

12. Hirota Y, Suzuki H, Nishimura Y, Yasuda S. 1977. On the process of cellular division in Escherichia coli: A mutant of *E. coli* lacking a murein-lipoprotein. Proc. Natl. Acad. Sci. USA. 74 (4), 1417-1420.

13. Matsuyama S, Tajima T, Tokuda H. 1995. A novel periplasmic carrier protein involved in the sorting and transport of Escherichia coli lipoproteins destined for the outer membrane. EMBO J. 14, 3365–3372.

14. Matsuyama SI, Yokota N, Tokuda H. 1997. A novel outer membrane lipoprotein, LolB (HemM), involved in the LolA (p20)-dependent localization of lipoproteins to the outer membrane of *Escherichia coli*. EMBO J. 16, 6947–6955.

15. Smith SG, Mahon V, Lambert MA, Fagan RP. 2007. A molecular Swiss army knife: OmpA structure, function and expression. FEMS Microbiol Lett. 273 (1), 1-11.

16. Marcoux J, Politis A, Rinehart D, Marshall DP, Wallace MI, Tamm LK2, Robinson CV. 2014. Mass spectrometry defines the C-terminal dimerization domain and enables modeling of the structure of full-length OmpA. Structure. 22 (5), 781-90.

17. Boags, A., Samsudin, F., Khalid, S. 2019. Binding from both sides: TolR and OmpA bind and maintain the local structure of the *E. coli* cell wall. Structure 27, 713-724

18. Mizuno T. 1979. A novel peptidoglycan-associated lipoprotein found in the cell envelope of Pseudomonas aeruginosa and Escherichia coli. J Biochem. 86 (4), 991-1000.

19. Lazzaroni JC, Portalier R. 1992. The excC gene of Escherichia coli K-12 required for cell envelope integrity encodes the peptidoglycan-associated lipoprotein (PAL). Mol Microbiol. 6 (6), 735-42.

20. Bontemps-Gallo S, Lacroix JM. 2015. New Insights into the Biological Role of the Osmoregulated Periplasmic Glucans in Pathogenic and Symbiotic Bacteria. Environ Microbiol Rep. 7 (5), 690–697.

21. Ruhal R, Kataria R, Choudhury B. 2013. Trends in bacterial trehalose metabolism and significant nodes of metabolic pathway in the direction of trehalose accumulation Microb. Biotechnol. 6(5), 493–502.

22. Wortham BW, Oliveira MA, Patel CN. 2007. Polyamines in Bacteria: Pleiotropic Effects Yet Specific Mechanisms, Adv Exp Med Biol, 603, 106-15.

23. Murarka A, Dharmadi Y, Yazdani SS, Gonzalez R. 2008. Fermentative Utilization of Glycerol by Escherichia coli and Its Implications for the Production of Fuels and Chemicals. Appl Environ Microbiol. 74 (4), 1124–1135.

24. Martínez-Gómez K. et al. 2012. New insights into Escherichia coli metabolism: carbon scavenging, acetate metabolism and carbon recycling responses during growth on glycerol. Microb Cell Fact. 11:46.

25. Beckers G, Bendt AK, Krämer R, Burkovski A. 2004. Molecular Identification of the Urea Uptake System and Transcriptional Analysis of Urea Transporter- and Urease-Encoding Genes in Corynebacterium glutamicum. J Bacteriol. 186 (22), 7645–7652.

719   26. Cayley DS, Guttman HJ, Record Jr MT. 2000. Biophysical Characterization of Changes
720   in Amounts and Activity of Escherichia Coli Cell and Compartment Water and Turgor
721   Pressure in Response to Osmotic Stress. Biophys J, 78 (4), 1748-64.
722   27. Boos, W. Ehmann U, Bremer E, Middendorf A, Postma P. 1987. Trehalase of
723   Escherichia coli. Mapping and cloning of its structural gene and identification of the
724   enzyme as a periplasmic protein induced under high osmolarity growth conditions. J Biol
725   Chem, 262 (27), 13212-8.
726   28. Cohen, S.S. 1997. A Guide to the Polyamines. Oxford University Press, New York, USA.
727   29. Shah P & Swiatlo E. 2008. A Multifaceted Role for Polyamines in Bacterial Pathogens.
728   Mol Microbiol, 68 (1), 4-16.
729   30. Wang D, Weng J, Wang W. 2019. Glycerol transport through the aquaglyceroporin GlpF:
730   bridging dynamics and kinetics with atomic simulation. Chem Sci, 10 (29), 6957-6965.
731   31. Krishnamurthy P. et al. 1998. Helicobacter pylori Containing Only Cytoplasmic Urease Is
732   Susceptible to Acid. Infect Immun. 66 (11), 5060–5066.
733   32. Lima MPM, Nader M, Santos DES, Soares TA. 2019. Compatibility of GROMOS-Derived
734   Atomic Parameters for Lipopolysaccharide Membranes with the SPC/E Water Model and
735   Alternative Long-Range Electrostatic Treatments Using Single Nonbonded Cutoff and
736   Atom-Based Charge Schemes. J. Braz. Chem. Soc. 30 (10), 2219-2230.
737   33. Berendsen, H. J., Postma, J. P. M., van Gunsteren, W. F. & Hermans, J. 1981. In
738   Intermolecular Forces (ed. Pullman, B.) 331–342 (Reidel Publishing, 1981).
739   34. Harada R, Sugita Y, Feig M. 2012. Protein Crowding Affects Hydration Structure and
740   Dynamics. J. Am. Chem. Soc. 134, 4842−4849.
741   35. von Bülow S, Siggel M, Linke M, Hummer G. 2019. Dynamic cluster formation
742   determines viscosity and diffusion in dense protein solutions. Proc Natl Acad Sci U S A.
743   116 (20), 9843-9852.
744   36. Yu I, Mori T, Ando T, Harada R, Jung J, Sugita Y, Feig M. 2016. Biomolecular
745   interactions modulate macromolecular structure and dynamics in atomistic model of a
746   bacterial cytoplasm. Elife. 5, e19274.
747   37. Bortot LO, Bashardanesh Z, van der Spoel D. 2020. Making Soup: Preparing and
748   Validating Models of the Bacterial Cytoplasm for Molecular Simulation. J. Chem. Inf.
749   Model. 60, 322−331.
750   38. Mullineaux CW, Nenninger A, Ray N, Robinson C. 2006. Diffusion of green fluorescent
751   protein in three cell environments in Escherichia coli. J. Bacteriol. 188 (10), 3442-3448.
752   39. Wallace et al. 2011. Self-assembly behaviour of colistin and its prodrug colistin
753   methanesulfonate: implications for solution stability and solubilization. J Phys Chem B.
754   114 (14), 4836–4840.
755   40. Ando T, Skolnick J. 2010. Crowding and hydrodynamic interactions likely dominate
756   in vivo macromolecular motion. Proc Natl Acad Sci USA. 107, 18457–18462.
757   41. Minton AP. 1980. Excluded volume as a determinant of protein structure and stability.
758   Biophys J. 32, 77–79.
759   42. Muramatsu N, Minton AP. 1989. Hidden self-association of proteins. J Mol Recognit.
760   1, 166–171.
761   43. Stradner A, et al. 2004. Equilibrium cluster formation in concentrated protein
762   solutions and colloids. Nature. 432, 492–495.

30

44. Paulino J, et al. 2019. Influenza A M2 channel clustering at high protein/lipid ratios: Viral budding implications. Biophys J. 116, 1075–1084.

45. Takeda et al. 2003. Crystal structures of bacterial lipoprotein localization factors, LolA and LolB. EMBO J. 22 (13), 3199–3209.

46. Koebnik R. 1995. Proposal for a peptidoglycan-associating *α*-helical motif in the C-terminal regions of some bacterial cell-surface proteins. Mol. Microbiol. 16, 1269–1270.

47. Parsons L.M., Lin F., Orban J. 2006. Peptidoglycan recognition by Pal, an outer membrane lipoprotein. Biochemistry. 45, 2122–2128.

48. Samsudin F, Boags A, Piggot TJ, Khalid S. 2017. Braun's Lipoprotein Facilitates OmpA Interaction with the Escherichia coli Cell Wall. Biophys. J. 113, 1496–1504.

49. Zaman, S. B. et al. 2017. A review on antibiotic resistance: alarm bells are ringing. Cureus, 9 (6), e1403.

50. Laxminarayan, R. et al. 2013. Antibiotic resistance: the need for global solutions. Lancet Infect. Dis. 13, 1057–1098.

51. Hobot JA, Carlemalm E, Villiger W, Kellenberger E. 1984. Periplasmic gel: new concept resulting from the reinvestigation of bacterial cell envelope ultrastructure by new methods. J Bacteriol. 160 (1), 143–152.

52. Pathania R. et al. 2009. Chemical genomics in Escherichia coli identifies an inhibitor of bacterial lipoprotein targeting. Nat. Chem. Biol. 5, 849–856.

53. Barker, C. A. et al. 2013. Degradation of MAC13243 and studies of the interaction of resulting thiourea compounds with the lipoprotein targeting chaperone LolA. Bioorg. Med. Chem. Lett. 23, 2426–2431.

54. Boags A, Samsudin F, Khalid S. 2019. Details of hydrophobic entanglement between small molecules and Braun's lipoprotein within the cavity of the bacterial chaperone LolA. Sci. Rep. 9, 3717.

55. Grabowicz M, Silhavy TJ. 2017. Redefining the essential trafficking pathway for outer membrane lipoproteins. Proc. Natl. Acad. Sci. U.S.A. 114, 4769–4774.

56. Caro F, Place NM, Mekalanos JJ. 2019. Analysis of lipoprotein transport depletion in Vibrio cholerae using CRISPRi. Proc Natl Acad Sci U S A. 116 (34), 17013-17022.

57. Tao K, Narita SI, Tokuda H. 2012. Defective Lipoprotein Sorting Induces lolA Expression through the Rcs Stress Response Phosphorelay System. J Bacteriol. 194 (14), 3643–3650.

58. Bontemps-Gallo S, Bohin JP, Lacroix JM. 2017. Osmoregulated Periplasmic Glucans. EcoSal Plus. 7 (2).

59. Mortensen, N. P. et al. 2009. Effects of colistin on surface ultrastructure and nanomechanics of Pseudomonas aeruginosa cells. Langmuir. 25, 3728-3733.

60. Konopka MC, Shkel IA, Cayley S, Record MT, Weisshaar JC. 2006. Crowding and confinement effects on protein diffusion in vivo. J Bacteriol. 188 (17), 6115-6123.

61. Schmid, N. *et al*. 2011. Definition and testing of the GROMOS force-field versions 54A7 and 54B7. Eur. Biophys. J. 40, 843–856.

62. van der Spoel D, van Maaren PJ, Berendsen HJC. 1998. A systematic study of water models for molecular simulation: Derivation of water models optimized for use with a reaction field. J. Chem. Phys. 108 (24), 10220-10230.

806 63. Petrov D, Zagrovic B. 2014. Are Current Atomistic Force Fields Accurate Enough to
807   Study Proteins in Crowded Environments? PLoS Comput Biol. 10 (5), e1003638.
808 64. Abriata LA, Dal Peraro M. 2015. Assessing the potential of atomistic molecular dynamics
809   simulations to probe reversible protein-protein recognition and binding. Scientific
810   Reports. 5, 10549.
811 65. Best, R. B.; Zheng, W.; Mittal, J. 2014. Balanced protein−water interactions improve
812   properties of disordered proteins and nonspecific protein association. J. Chem. Theory
813   Comput. 10, 5113−5124.
814 66. Carballo-Pacheco, M.; Ismail, A. E.; Strodel, B. 2018. On the Applicability of Force Fields
815   to Study the Aggregation of Amyloidogenic Peptides Using Molecular Dynamics
816   Simulations. J. Chem. Theory Comput. 14, 6063−6075.
817 67. Samsudin F, Ortiz-Suarez ML, Piggot TJ, Bond PJ, Khalid S. 2016. OmpA: A Flexible
818   Clamp for Bacterial Cell Wall Attachment. Structure 24, 2227–2235.
819 68. Piggot TJ, Holdbrook DA, Khalid S. 2011. Electroporation of the E. coli and S. Aureus
820   membranes: molecular dynamics simulations of complex bacterial membranes. J. Phys.
821   Chem. 115, 13381–8.
822 69. Ortiz-Suarez ML, Samsudin F, Piggot TJ, Bond PJ, Khalid S. 2016. Full-Length OmpA:
823   Structure, Function, and Membrane Interactions Predicted by Molecular Dynamics
824   Simulations. Biophys. J. 111, 1692–1702.
825 70. Shu W, Liu J, Ji H, Lu M. 2000. Core structure of the outer membrane lipoprotein from
826   Escherichia coli at 1.9 A resolution. J. Mol. Biol. 299, 1101–1112.
827 71. Bonsor, D. A. et al. 2009. Allosteric beta-propeller signalling in TolB and its manipulation
828   by translocating colicins. EMBO J. 28, 2846–2857.
829 72. Szczepaniak J. et al. 2020. The lipoprotein Pal stabilises the bacterial outer membrane
830   during constriction by a mobilisation-and-capture mechanism. Nat Comm. 11, 1305.
831 73. Horta, B.A.C., Fuchs, P.F.J., van Gunsteren, W.F., and Hunenberger, P.H. 2011. New
832   interaction parameters for oxygen compounds in the GROMOS force field: improved
833   pure-liquid and solvation properties for alcohols, ethers, aldehydes, ketones, carboxylic
834   acids, and esters. J. Chem. Theor. Comput. 7, 1016–1031.
835 74. Koziara KB, Stroet M, Alpeshkumar MK, Mark AE. 2014. Testing and validation of the
836   Automated Topology Builder (ATB) version 2.0: prediction of hydration free enthalpies. J.
837   Comput. Aided Mol. Des. 28, 221–233.
838 75. Wolf MG. *et al*. 2010. g_membed: efficient insertion of a membrane protein into an
839   equilibrated lipid bilayer with minimal perturbation. J. Comput. Chem. 31, 2169–2174.
840 76. Plazinski W, Lonardi A, Hünemberger PH. 2016. Revision of the GROMOS
841   56A6(CARBO) Force Field: Improving the Description of Ring-Conformational Equilibria
842   in Hexopyranose-Based Carbohydrates Chains. J Comput Chem. 37 (3), 354-365.
843 77. Abraham, M. J. *et al*. 2015. GROMACS: High performance molecular simulations
844   through multi-level parallelism from laptops to supercomputers. SoftwareX. 1, 19–25.
845 78. Bussi, G., Donadio, D. & Parrinello, M. 2007. Canonical sampling through velocity
846   rescaling. J. Chem. Phys. 126, 014101.
847 79. Parrinello, M., Rahman, A. 1981. Polymorphic transitions in single crystals: A new
848   molecular dynamics method. J. Appl. Phys. 52, 7182.

849   80. Darden, T., York, D. & Pedersen, L. 1993. Particle mesh Ewald: An N·log(N) method for
850   Ewald sums in large systems. J. Chem. Phys. 98, 10089–10092.
851   81. Hess, B., Bekker, H., Berendsen, H. J. C. & Fraaije, J. G. E. M. 1997. LINCS: A linear
852   constraint solver for molecular simulations. J. Comp. Chem. 18, 1463–1472.
853   82. Hess, B. 2008. P-LINCS: A Parallel Linear Constraint Solver for Molecular Simulation. J.
854   Chem. Theory Comput. 4, 116-122.
855   83. Humphrey, W. & Dalke, A. 1996. VMD: visual molecular dynamics. J. Mol. Graph. 15,
856   33–38.

857
858
859
860
861
862
863
864   **For Table of Contents Only**
865